

# Low Second-Harmonic Content in Transformer Inrush Currents – Analysis and Practical Solutions for Protection Security

Steven Hodder

*Hydro One Networks, Inc.*

Bogdan Kasztenny, Normann Fischer, and Yu Xia

*Schweitzer Engineering Laboratories, Inc.*

© 2014 IEEE. Personal use of this material is permitted. Permission from IEEE must be obtained for all other uses, in any current or future media, including reprinting/republishing this material for advertising or promotional purposes, creating new collective works, for resale or redistribution to servers or lists, or reuse of any copyrighted component of this work in other works.

This paper was presented at the 67th Annual Conference for Protective Relay Engineers and can be accessed at: <http://dx.doi.org/10.1109/CPRE.2014.6799037>.

For the complete history of this paper, refer to the next page.

Presented at the  
Southern African Power System Protection Conference  
Johannesburg, South Africa  
November 12–14, 2014

Previously presented at the  
68th Annual Georgia Tech Protective Relaying Conference, April 2014,  
and 67th Annual Conference for Protective Relay Engineers, March 2014

Previous revised edition released October 2013

Originally presented at the  
40th Annual Western Protective Relay Conference, October 2013

# Low Second-Harmonic Content in Transformer Inrush Currents – Analysis and Practical Solutions for Protection Security

Steven Hodder, *Hydro One Networks, Inc.*

Bogdan Kasztenny, Normann Fischer, and Yu Xia, *Schweitzer Engineering Laboratories, Inc.*

**Abstract**—This paper addresses the security of transformer differential protection with low levels of second harmonic during magnetizing inrush conditions. The paper explains the phenomenon of ultrasaturation causing the second harmonic to drop below the traditional 15 to 20 percent setting levels and points to possible causes of and conditions for ultrasaturation. A number of field cases are presented and discussed in addition to the engineering analysis of the problem. The paper outlines several simple solutions to address the security problem while minimizing the adverse impact on dependability. Further, the paper presents a new method for inrush detection that considerably improves security without diminishing dependability. Finally, a method to accelerate operation of transformer differential protection is presented.

## I. INTRODUCTION

Power transformers rated above 5 to 10 MVA are typically protected with differential (87T) elements against internal short circuits. The 87T differential (operating) signal is based on the ampere-turn balance equations of the protected transformer [1]. As such, it responds to transformer faults and balances out to zero for load and all external faults. Unfortunately, the 87T differential signal also reflects the transformer magnetizing current during inrush and overexcitation conditions. This is because the magnetizing branch in the transformer model is a shunt diverting the current away from the differential measurements.

Transformer inrush currents can be large, in the order of five to seven times the transformer rated current, and they would normally cause the 87T element to misoperate if not properly blocked or restrained. Inrush currents are typically rich in harmonics, the second harmonic in particular. Therefore, the second-harmonic content in the differential currents has been traditionally used in transformer differential elements to block or to increase restraint during inrush conditions.

However, some power transformers, especially new designs with the core material improved for lower losses but also older units under some conditions, produce low levels of second harmonic in their magnetizing currents during energization. As a result, their 87T elements face security problems when the second harmonic falls below the traditional 15 or 20 percent second-harmonic setting levels.

We show in this paper that low second harmonic is caused by deep saturation (sometimes called ultrasaturation) of the transformer core. During ultrasaturation, the transformer core is operated at very high levels of flux, and as a result, the magnetizing current-flux operating point traverses along the transformer magnetizing curve in the saturated portion of the characteristic. This, in turn, makes the core appear more linear, as if it had only the saturated portion of the magnetizing curve. This linearity decreases the harmonic content in the inrush currents—sometimes well below 10 percent—causing security problems for transformer differential protection.

This paper explains the ultrasaturation phenomenon and illustrates it with actual field cases. Further, this paper presents practical solutions to this protection security problem, ranging from simple setting and logic choices to a new method of detecting magnetizing inrush with enhanced security during transformer ultrasaturation.

## II. TRANSFORMER INRUSH CURRENTS

### A. Physics of Transformer Inrush

For simplicity, we use a single-phase transformer model in our analysis, as shown in Fig. 1.

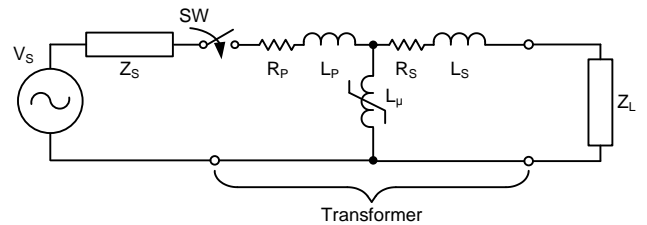


Fig. 1. Single-phase equivalent circuit used for analysis of transformer energization.

As can be seen from Fig. 1, the magnetizing branch—an intrinsic part of the transformer—is represented by a nonlinear inductor with a magnetic characteristic as shown in Fig. 2. As we will see, it is the magnetic characteristic of the transformer core that primarily dictates the magnitude of the inrush current when the transformer is energized.

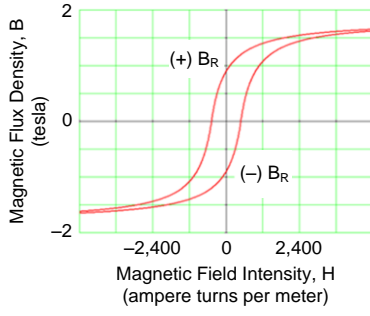


Fig. 2. B-H curve of a typical transformer.

Fig. 2 is referred to as the B-H curve of the transformer core (magnetic material) and is a plot of the magnetic flux density ( $B$ ) of the core as a function of the magnetic field intensity ( $H$ ). From Fig. 2, we see that at some point, increasing the magnetic field intensity does not result in an increase in the magnetic flux density. At this point, all the magnetic domains of the transformer core material are aligned with the magnetic field and we say that the transformer core is saturated. How does the transformer core being saturated impact the inrush current? To answer this question, we examine the equation used to calculate the inductance of the magnetizing branch of the transformer core ( $L_\mu$ ):

$$L_\mu = \frac{N^2 A \mu_0 \mu_r}{l} \quad (1)$$

In (1), we notice that the inductance is directly proportional to the number of turns ( $N$ ), the area of the core ( $A$ ), and the permeability of the material ( $\mu_0 \mu_r$ ). It is inversely proportional to the length of the core ( $l$ ). Of these,  $N$ ,  $A$ , and  $l$  are constant, while the permeability of the material depends on the operating point on the B-H curve and can be obtained as follows:

$$\mu_0 \mu_r = \frac{B}{H} \quad (2)$$

From Fig. 2, we can see that for lower levels of  $B$  and  $H$ ,  $B$  and  $H$  change proportionally with each other. However, when  $H$  reaches a certain point (known as saturation), a large increase in  $H$  results in a very small change in  $B$ . Beyond this point, the ratio of  $B$  to  $H$  trends toward zero, meaning that the permeability of the material (in this case, the transformer core) trends toward zero. Fig. 3 is a plot of the relative permeability for the magnetic material of Fig. 2 (we can see how the relative permeability [ $\mu_r$ ] decreases as  $H$  increases).

If we now relate Fig. 3 to (1), we can see that as  $H$  increases, the inductance of the magnetizing impedance ( $L_\mu$ ) of the transformer decreases because the relative permeability of the magnetic material ( $\mu_r$ ) decreases with  $H$ .

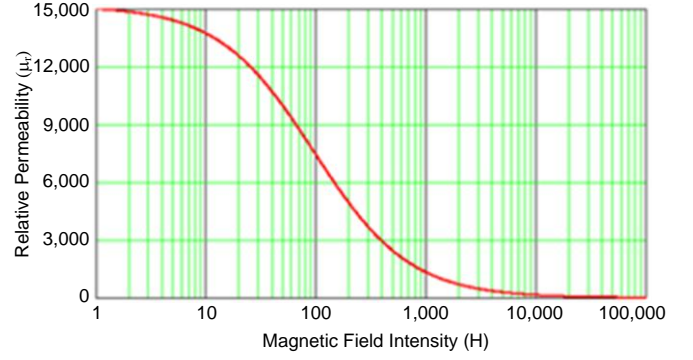


Fig. 3. Relative permeability ( $\mu_r$ ) versus the magnetic field intensity ( $H$ ).

### B. Magnetizing Inrush Current Characteristic

To see how this change in the magnetizing impedance affects the inrush current of a transformer, we close the switch (SW) in Fig. 1 at time  $t_0$  when the voltage of the source is crossing zero in the positive direction. The voltage across the magnetizing branch (inductor  $L_\mu$ ) gives rise to flux ( $\psi$ ) with the following relationship:

$$\psi = \frac{1}{N} \int v dt \quad (3)$$

The flux affects the relative permeability of the magnetic material of the magnetizing branch, which, in turn, determines the inductance of this branch. The magnetizing branch inductance controls the current drawn by the transformer during energization (see Fig. 4).

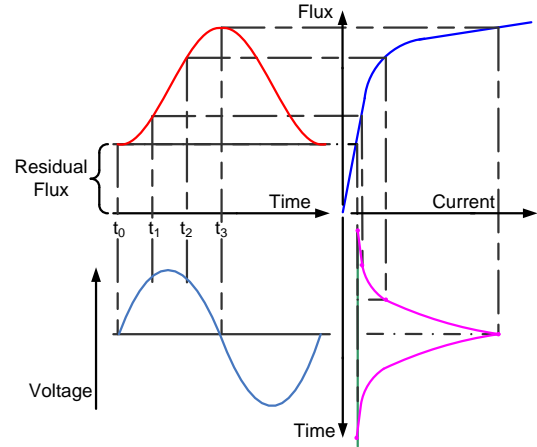


Fig. 4. Magnetizing voltage, core flux, and magnetizing current relationship in a transformer.

From Fig. 4, we can make the following observations. When the transformer is energized ( $t_0$ ), the instantaneous voltage is zero. However, the flux at this instant is not zero but at the residual flux value ( $B_R$ ), as shown in Fig. 2. At this time, the relative permeability is still high ( $\mu_r \approx 8,000$ );

therefore, the magnetizing branch (as shown in Fig. 1) presents a large inductance and the transformer draws a relatively low magnetizing (excitation) current. As the instantaneous voltage increases ( $t_1$ ), so does the flux (the instantaneous voltage is still positive). Because the flux is still in the linear region of the B-H curve, the relative permeability stays approximately the same and the instantaneous current increases linearly with the voltage. While the instantaneous voltage is positive, the flux continues to increase, reaching its maximum value at the negative voltage zero crossing ( $t_3$ ). However, as the flux increases ( $t_2$ ), the relative permeability of the magnetizing branch will begin to decrease. This decrease in relative permeability causes the magnetizing branch inductance to decrease, resulting in a larger current being drawn from the source. When the flux has reached its maximum value ( $t_3$ ), the relative permeability is at its lowest point, and as a result, the inductance of the magnetizing branch is at its lowest value. If at this point the relative permeability approaches zero, the impedance of the magnetizing branch will also tend to zero. As the impedance of the magnetizing branch tends to zero, the current drawn by the transformer at this point is practically limited only by the source impedance ( $Z_S$ ) and the relatively small leakage inductance and winding resistance of the transformer ( $R_P + jX_P$ ). As can be seen in Fig. 5, the magnetizing branch is effectively short-circuited at this point.

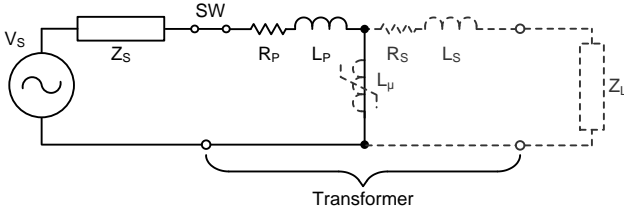


Fig. 5. Single-phase equivalent circuit used for analysis of transformer energization: the case of a deeply saturated core.

We can therefore conclude that the energization current drawn by a transformer is determined by the flux (which is proportional to the flux density), which, in turn, is determined by the voltage applied to the transformer and the residual flux ( $B_R$ ) present when the transformer is energized. The point on the voltage wave at which the transformer is energized also plays an important role in that the flux produced is dependent on the integral of the instantaneous voltage (3). It can be easily understood that the maximum flux will be developed when the transformer is energized on the positive zero crossing of the voltage wave if the transformer has a positive residual flux (this is because during the first half cycle, the voltage will be positive and this will cause the flux to increase). Energizing the transformer at a later point on the voltage waveform results in a smaller flux increase, resulting in a smaller maximum flux.

The source impedance plays another important role in that it not only determines the peak magnitude of the inrush current (see Fig. 5) but it also determines the duration (decay rate) of the inrush current. This can be easily understood when examining Fig. 5. When the magnetizing branch is short-circuited, the remaining circuit basically contains only

the transformer winding resistance and leakage inductance ( $R_P$  and  $L_P$ ) and the source impedance ( $Z_S$ ). Generally, the source impedance is much larger than the transformer leakage impedance, and therefore, the time constant of the transformer energization (inrush) current is basically the time constant of the source ( $L/R$  of the source).

The energization current of a transformer is determined by the following three factors:

- The residual flux in the transformer core ( $B_R$ ).
- The point on the wave of the voltage at which the transformer is energized.
- The magnitude of the source impedance and, to a smaller degree, the magnitude of the transformer leakage impedance.

### C. The Role of B-H Loops During Energization

Assume that the residual flux is positive [ $(+)$   $B_R$  in Fig. 2]. If at the time that the transformer is energized the voltage is going through a positive zero crossing, the flux developed by the voltage and the residual flux will both be positive and the positive voltage will cause the flux to increase. If we plot the flux developed in the transformer core versus the magnetic field intensity (as a function of the current drawn by the transformer), we obtain a plot as shown in Fig. 6. It can be observed that the first loop (1 in Fig. 6) traverses a much smaller area than the second, third, and consecutive loops on the B-H plane.

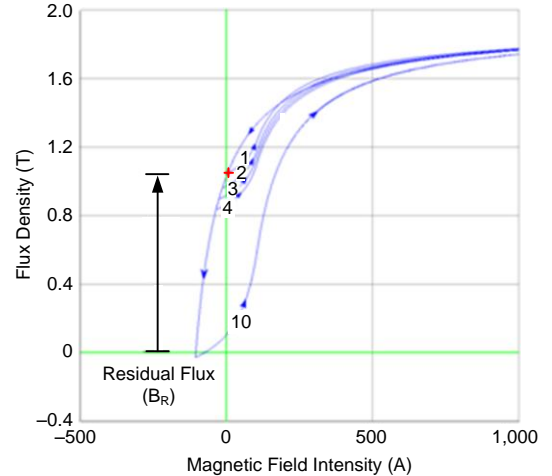


Fig. 6. Trajectory of the flux density ( $B$ ) versus the magnetic field intensity ( $H$ ) during transformer energization.

When the switch is initially closed (see Fig. 1), the voltage across the magnetizing branch ( $L_\mu$ ) is approximately equal to the source voltage. As the voltage increases, the voltage across the magnetizing branch increases proportionally and, as a result, so does the flux in the transformer core. As the voltage continues to increase, the flux in the transformer core increases; however, the relative permeability of the core begins to decrease, causing the inductance of the magnetizing branch to decrease as well. As a result of  $L_\mu$  decreasing, the voltage drop across the magnetizing branch begins to decrease and so does the flux developed by the voltage. However, because the voltage across the magnetizing branch is still

positive, the flux continues to increase but at a lower rate because the voltage is now lower. The increase in flux results in a further decrease in the relative permeability, which results in an even lower voltage across  $L_{\mu}$ .

Fig. 7 is a plot of the voltage across the magnetizing branch during energization. As the transformer goes into saturation, the voltage across the magnetizing branch ( $L_{\mu}$ ) decreases. The result of this is that the flux in the transformer core cannot reach the maximum value corresponding to the source voltage (see Fig. 8). When the voltage becomes negative, the flux in the core begins to decrease, and as a result, the inductance of the transformer core begins to become reestablished, allowing the voltage magnitude across the core to increase, this time in the negative direction.

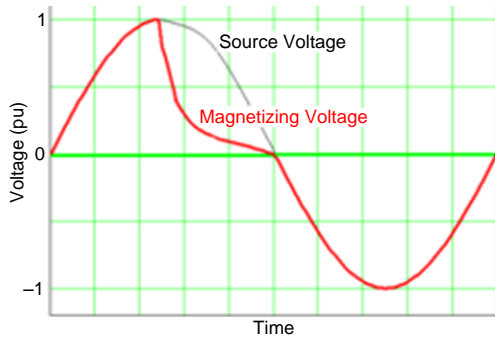


Fig. 7. Source and transformer voltage during energization.

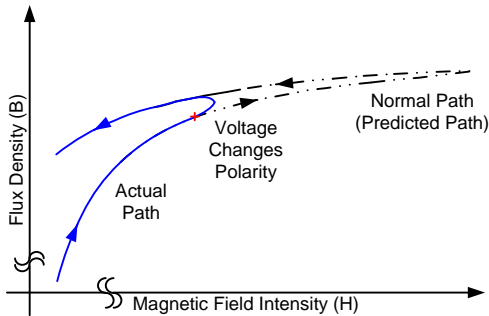


Fig. 8. B-H trajectory for the first voltage cycle (the flux developed in the core does not reach its full potential).

Because the core does not go into saturation when the voltage has a negative polarity, the voltage across the magnetizing branch is approximately equal to that of the source, and this allows a larger negative flux to be developed. The flux developed during the negative half cycle of the voltage is therefore larger than the flux developed during the positive half cycle. As a result, when the voltage goes positive again, the flux in the transformer core is lower than what it was when the transformer was energized a cycle earlier.

This process continues in the next positive half cycle, and again the developed flux is less than the flux developed during the negative half cycle. As a result, the transformer gradually comes out of saturation and the magnetizing current begins to decrease.

Note that the consecutive loops of the B-H trajectory, as shown in Fig. 6, decay relatively slowly. If the transformer

were to be tripped within the first few cycles into energization, the residual flux would stay at relatively high levels even if the initial residual flux was low. This is true because the B-H operating point follows the major loop on its way toward lower values of  $H$ . This observation helps us when analyzing cases of deep saturation due to restrikes (Section IV).

#### D. Harmonic Content in the Inrush Currents

In examining the profile of the energization current in Fig. 4, we see that the shape of the current wave is unipolar. Therefore, we expect the energization current to be rich in even harmonics. Fig. 9 is a plot of a phase current and its harmonics during energization of a three-phase transformer. We can see that the predominant harmonic during transformer energization is the second harmonic. Also present are the third, fourth, and fifth harmonics.

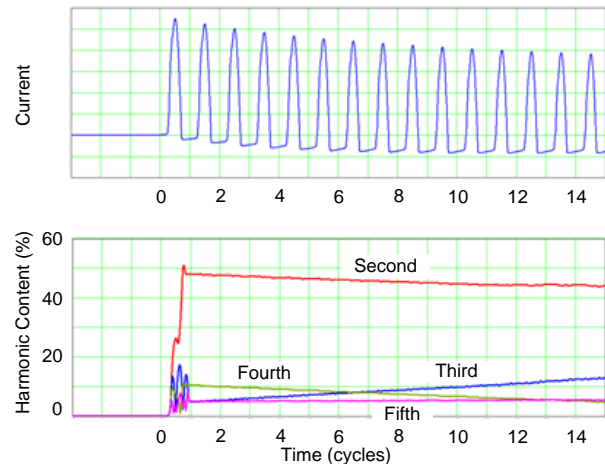


Fig. 9. Transformer terminal phase current during energization (top) and the percentage harmonic content of the phase current during this time period (bottom).

#### E. Dwell-Time Intervals in the Inrush Currents

As illustrated in Fig. 10, the magnetizing currents of a three-phase transformer (available as the differential signals to the 87T element) exhibit intervals where the currents are both small and flat. These periodic intervals have been observed to last at least one-sixth of a power cycle.

This observation was used in some early implementations of the dwell-time principle (waveform analysis) in differential relays. We analyze this principle and considerably improve it in Section VI.

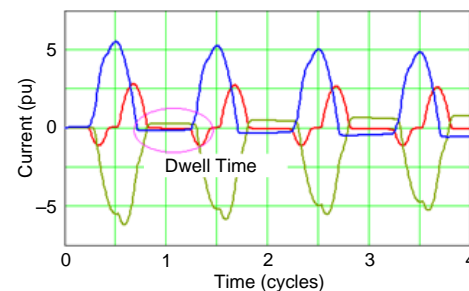


Fig. 10. Dwell-time intervals in the inrush currents.

### F. DC Area Ratio

As illustrated in Fig. 9 and Fig. 10, the areas below the positive portions of the current wave and the negative portions of the current wave are different. This is because the inrush current is greatly offset when it is large. As a result, the ratio of the positive-to-negative areas is either much smaller or much greater than 1. This observation facilitates one possible method (dc blocking logic) of providing security during inrush conditions [2].

### G. Harmonic Blocking/Restraining in 87T Elements

By the principle of differential protection, the magnetizing currents of the transformer are measured as differential signals of the 87T elements. This is not desirable, but it cannot be avoided and it needs to be dealt with because the inrush currents can be relatively large.

To secure the differential element during transformer energization, the harmonic content of the corresponding phase differential current is used. In harmonic blocking schemes, the differential element is blocked from operating if the percentage of the harmonic content of the differential current is greater than a preset value, typically 15 to 20 percent of the fundamental (see Fig. 11a). In harmonic restraint schemes, the harmonic content of the differential current is used to boost the restraint current (the harmonic content in the differential current is added to the restraint current) to prevent the differential element from operating (see Fig. 11b).

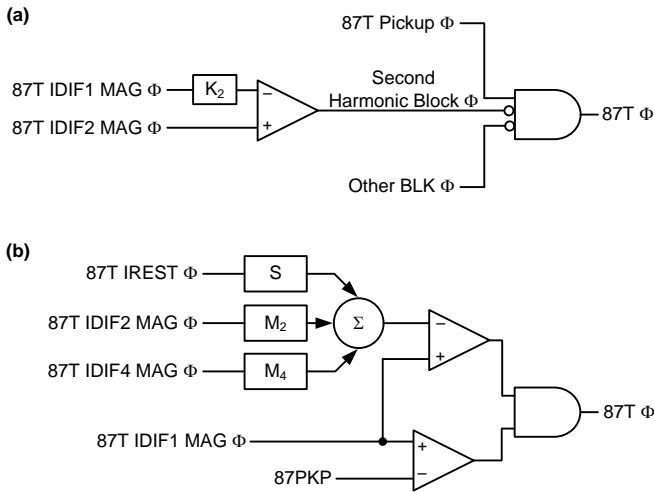


Fig. 11. The principles of harmonic blocking (a) and restraining (b).

The question that can be asked now is which harmonic should be used to block or restrain the differential element. No third- or triplen-harmonic currents can be used to block or restrain the differential element during energization because these harmonics are of the zero-sequence symmetry and therefore are effectively removed from the differential signals [1]. However, the second harmonic (which is of the negative-sequence symmetry) and the fourth harmonic (which is of the positive-sequence symmetry) are preserved in the differential currents. As such, they can be used to block or restrain the differential element.

In a harmonic blocking scheme, if the percentage of second- or fourth-harmonic current is greater than a set pickup (usually a value not lower than about 15 percent of the fundamental), the differential element is blocked.

In a harmonic restraining scheme, the second- and fourth-harmonic currents are used to boost the restraint quantity, contributing to the security of the differential element.

### H. Impact of Current Transformers on Inrush Current Measurements

Current transformers (CTs) are used to measure the phase terminal currents of the transformer. Having magnetic cores themselves, CTs are subject to the same physics of saturation as the power transformer. Fig. 9 is the secondary terminal phase current for a transformer being energized. This current is a very slowly decaying, predominantly unipolar waveform, or stated differently, it contains a slowly decaying dc offset superimposed on a decaying oscillating component. The result of this very slowly decaying dc offset is that the CT may be eventually driven into saturation. When a CT is operated in the saturation mode, it no longer produces a true replica of the primary current. The first sign of CT saturation is that the dwell-time intervals display a current that is gradually increasing and becoming gradually tilted (see Fig. 9 and Fig. 10). We explain the phenomenon of CT ultrasaturation in Section IV.

## III. EXAMPLES OF LOW SECOND HARMONIC IN TRANSFORMER INRUSH CURRENTS

Cases of sporadic misoperation of transformer protection during inrush conditions are reported, with the common cause of the second-harmonic ratio being too low to properly block or restrain the differential element.

### A. Transformer Energization

Fig. 12 shows a sample inrush current during relay misoperation due to a low second harmonic. The Phase C current is the largest, but it has second-harmonic content well below 15 percent of the fundamental, considered the lowest setting that does not impair dependability (Fig. 13).

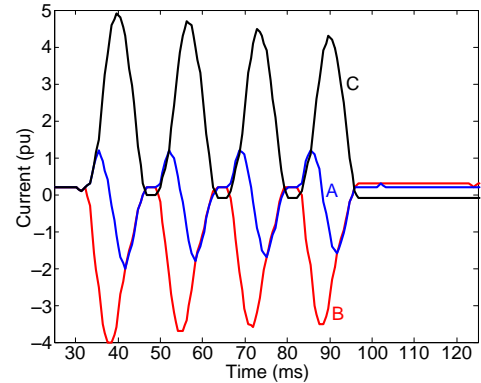


Fig. 12. Sample inrush terminal currents during energization.

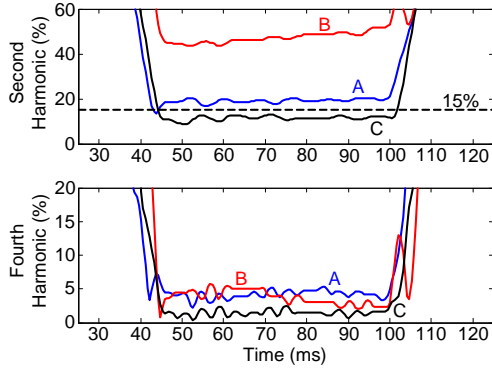


Fig. 13. Second- and fourth-harmonic content in the terminal currents of Fig. 12.

Fig. 12 and Fig. 13 relate to the transformer terminal currents. Would vector group compensation alter the harmonic content? Consider Phase A (delta connection) compensation, as follows (similar equations apply to Phase B and Phase C differential currents [1]):

$$i_{\text{DIF-A}} = \frac{1}{\sqrt{3}}(i_A - i_B) \quad (4)$$

Fig. 14 and Fig. 15 show the instantaneous differential currents and their harmonic content, respectively, for the case of Fig. 12.

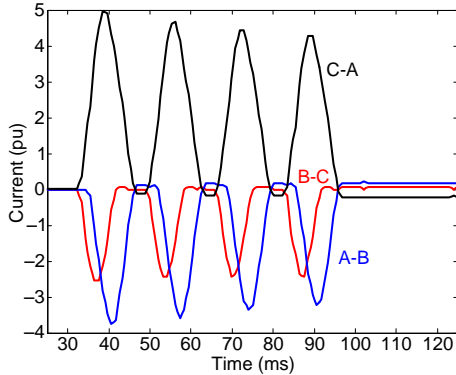


Fig. 14. Differential currents for the case of Fig. 12, assuming delta compensation (CT connection).

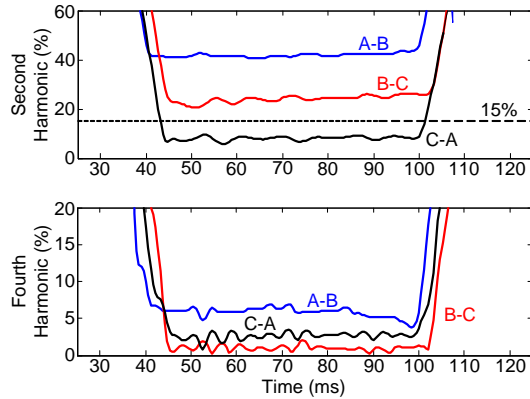


Fig. 15. Second- and fourth-harmonic content in the differential currents of Fig. 14.

Equation (4) applies to instantaneous values and therefore is the equivalent of subtracting phasors as vectors. The fundamental frequency phasors subtract as vectors, as do the

second- and fourth-harmonic phasors. As a result, the fundamental frequency and the second- and fourth-harmonic phasors in the differential currents can increase or decrease (as compared with the terminal currents) depending on their relative angles between phases. Consider the terminal currents of Fig. 12—their harmonic content is about 20, 50, and 10 percent in Phases A, B, and C, respectively. The differential currents of Fig. 14 have the harmonic content of 50 percent (A-B), 25 percent (B-C), and 10 percent (C-A). The harmonic content of Fig. 15 shows that the Phase C differential (C-A) still reads low while the other two differential elements have sufficient second-harmonic levels. As illustrated, the low second-harmonic problem does not go away nor is introduced by applying vector group compensation.

Would harmonic restraining work better than harmonic blocking for this case? Refer to Fig. 11b, and assume a slope of 40 percent ( $S = 0.4$ ). In order to restrain the relay from the second harmonic only with the equivalent level of 15 percent,

the  $M_2$  multiplier would have to be  $\frac{(1-0.4)}{0.15} = 4$ . Note that

under inrush, the restraint current equals the differential current ( $87T \text{ IREST} = 87T \text{ DIF1 MAG}$ ). Therefore, we get the total restraint equal to  $0.4 \cdot (87T \text{ DIF1 MAG}) + 4 \cdot (0.15 \cdot 87T \text{ DIF1 MAG}) = 87T \text{ DIF1 MAG}$ , and the comparator in Fig. 11b would be at the border of operating.

However, as shown in Fig. 15, the Phase C second harmonic reads only about 10 percent while the Phase C fourth harmonic reads only about 2 percent. With 10 percent of the second harmonic, the total restraint would be  $0.4 \cdot (87T \text{ DIF1 MAG}) + 4 \cdot (0.10 \cdot 87T \text{ DIF1 MAG}) = 0.8 \cdot (87T \text{ DIF1 MAG})$  and the element would misoperate.

To produce the missing  $0.2 \cdot (87T \text{ DIF1 MAG})$  of the restraint from the 2 percent of the fourth harmonic, the  $M_4$  multiplier would have to be  $\left(\frac{0.2}{0.02}\right) = 10$ .

With high enough multiplier values, we could stabilize the 87T element. However, assume an internal single-end feed fault with CT saturation that produces 10 percent of the fourth harmonic. With the  $M_4$  multiplier of 10, the fourth harmonic would produce an extra restraint of  $0.10 \cdot 10 \cdot 87T \text{ DIF1 MAG} = 87T \text{ DIF1 MAG}$  and would incorrectly restrain the relay from operating (loss of dependability).

Therefore, increasing the  $M_4$  multiplier too high to cover for the low level of second harmonic during inrush conditions is not recommended.

As illustrated, both the blocking and restraining algorithms may exhibit security problems under inrush conditions with low levels of harmonics.

### B. Switching Device Restrike

Another scenario that can lead to transformer protection security problems is a restrike when de-energizing an unloaded transformer, particularly via a motor-operated disconnect switch.

Fig. 16 shows an operation of de-energizing a power transformer tapped from a transmission line with a disconnect

switch. The figure shows a repetitive pattern of inrush current that flows when the switch conducts and ceases to flow when the air insulation is sufficient to extinguish the arc. Note that the magnitude of the current on the second restrike is higher than on the first restrike. At the same time, the harmonic content is lower on the second restrike (see Fig. 17).

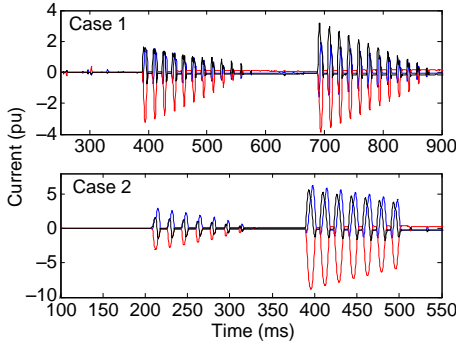


Fig. 16. Sample inrush current due to restrike during disconnect switch opening (two different cases).

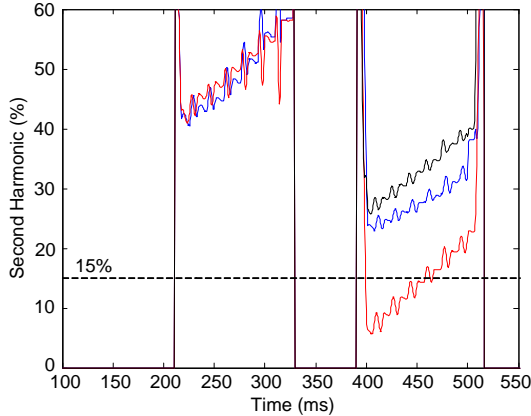


Fig. 17. Second-harmonic content in currents of Fig. 16 (Case 2).

After several restrikes, the transformer core goes into deeper saturation, generating higher inrush currents and potentially lower second-harmonic levels. At the same time, the polarity of the currents can be consistent between the restrikes. Prolonged restriking with unipolar currents subjects the CTs to a long-lasting dc component. This dc component does not have a chance to fully decay, but it restarts from the initial inrush value each time the switch starts to conduct again. The initial current value on each restrike is high and depends on the residual flux in the transformer core and the system impedance, as explained in Section II. This is likely to drive the CTs into saturation as the CT flux accumulates because of the high and unipolar values of the current.

Fig. 18 illustrates this phenomenon, presenting a simulated case of restrike. As we can see, the secondary waveform shows known symptoms of subsidence current distorting the dwell-time periods and making the waveform smoother.

We return to the analysis of inrush when restriking and the issue of CT saturation in Section IV.

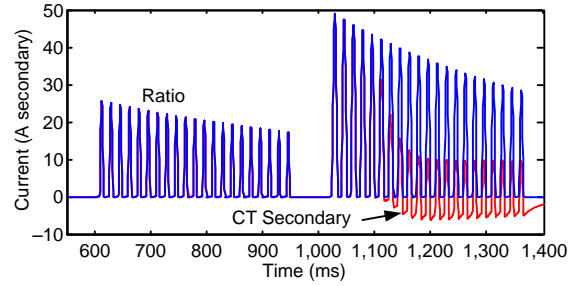


Fig. 18. Ratio (blue) and CT secondary (red) currents during a restrike (computer simulation).

From the field cases presented in this section, we can draw the conclusion that the second-harmonic content in the differential currents becomes low when the transformer core is driven into deep saturation. This phenomenon is often referred to as ultrasaturation. We explain and characterize ultrasaturation in the next section.

#### IV. ULTRASATURATION IN TRANSFORMERS

##### A. Explanation of Ultrasaturation

The phenomenon of ultrasaturation can be explained by assuming a magnetizing characteristic with two linear regions, as shown in Fig. 19 through Fig. 22, and applying a sine-wave-shaped flux in the core with the magnitude below the saturation level while varying the amount of residual flux.

When the residual flux is near zero, the flux oscillates between the positive and negative saturation points and the transformer works in the linear region of operation, drawing only a very small excitation current, as shown in Fig. 19. In the simplified model of Fig. 19, the current is sinusoidal because we assumed a perfectly linear magnetizing characteristic. In reality, this current is heavily distorted with large amount of odd harmonics, the fifth harmonic in particular because the current-flux characteristic is nonlinear near the zero flux point (see Fig. 4).

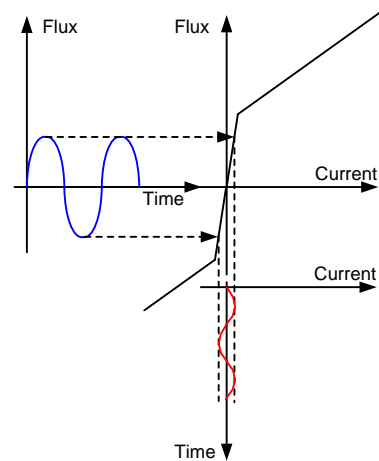


Fig. 19. Current and flux in the case when flux oscillates between the negative and positive saturation levels.

Assume next that the transformer is energized with some amount of residual flux, as shown in Fig. 20. The sine-wave flux is shifted in such a way that the maximum flux is in the second slope of the magnetizing characteristic. When the flux is above the saturation point, the transformer draws a large magnetizing current, as explained in Section II. We assume, however, that the minimum flux is below the saturation point. When the flux is below the saturation level, the transformer draws a very small current. This switching between the large and small current in every power system cycle results in a typical shape of the inrush current with large values of the same polarity separated by periods of very small current (dwell-time periods), as shown in Fig. 20. As explained in Section II, this is a typical case of saturation during magnetizing inrush conditions. The current is excessive, typically well above the transformer nominal current and the pickup level of transformer differential protection. A sufficient amount of second harmonic is present, however, allowing the differential elements to be properly blocked or restrained.

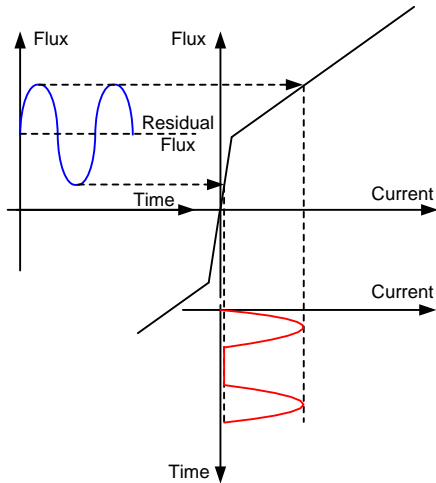


Fig. 20. Current and flux in the case when the maximum flux is above the saturation level and the minimum flux is below the saturation level.

Assume now that the residual flux is high so that the minimum flux is below the saturation level for only a very short period of time, as depicted in Fig. 21. In this case, the dwell-time periods are proportionally shorter and the current waveform appears closer to a sine wave, showing lower levels of harmonics.

Fig. 22 presents an ultimate case when the flux is pushed above the saturation point so that even the minimum flux is above the saturation level. In this situation, the transformer draws a very large current, but the current waveform is not distorted. The transformer core is operated in the saturated region, but the magnetizing inductance, even though low, is constant, thereby yielding a current that is similar to a sine wave [see Fig. 3 and (1)]. This case is referred to as ultrasaturation.

Because the current waveform is relatively undistorted during ultrasaturation, the harmonic content is extremely low, thus jeopardizing the security of transformer differential protection.

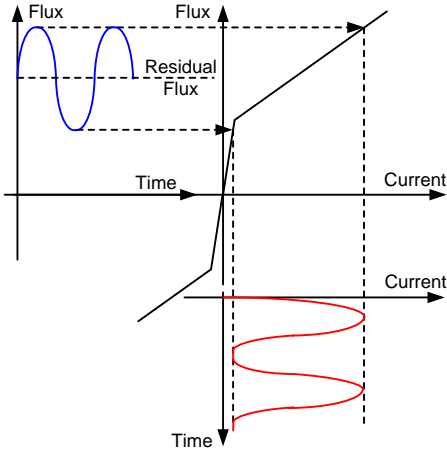


Fig. 21. Current and flux in the case when the minimum flux is close to the saturation level.

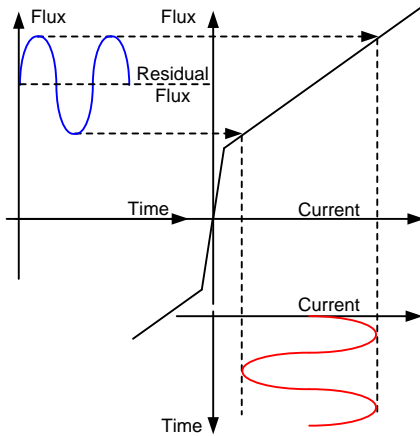


Fig. 22. Current and flux in the case when both the maximum and minimum flux values are above the saturation level.

Fig. 23 illustrates the low second-harmonic content by plotting the percentage of second harmonic as a function of residual flux for the simplified cases shown in Fig. 19 through Fig. 22. When the residual flux increases slightly so that the transformer core starts saturating, the second-harmonic content increases considerably (right of Point A on the curve in Fig. 23). Below that level of flux, the magnetizing current is very low (steady-state excitation current rather than a transient inrush current) and the second-harmonic blocking or restraining action is not needed.

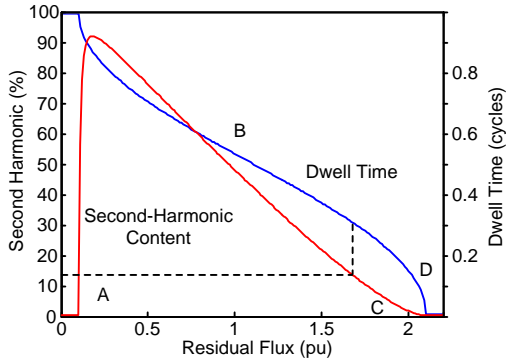


Fig. 23. Second-harmonic content (red) and duration of the dwell time (blue) as a function of residual flux. Point A is the case shown in Fig. 19, Point B is the case shown in Fig. 20, Point C is the case shown in Fig. 21, and Point D is the case shown in Fig. 22.

As the level of residual flux increases, the oscillating flux is pushed further into the saturation region, resulting in increased second-harmonic content (up to about 90 percent in our example). However, as the residual flux increases even more, the operating point of the flux versus current traverses greater portions of the second slope of the B-H characteristic, resulting in a more sinusoidal shape of the current with the decreasing second-harmonic content. The case of Fig. 21 results in roughly only 10 percent second-harmonic content (Point C in Fig. 23). The moment the oscillating flux is entirely pushed into the second slope region, the second harmonic decreases to extremely low values—eventually zero (Point D in Fig. 23).

From this explanation, we can see that ultrasaturation is a consequence of pushing the oscillating flux deeply into the saturated portion of the magnetizing characteristic, to the point when even the minimum flux level is near or even beyond the saturation point. Under such conditions, the magnetizing current is very large but is not distorted; therefore, it is low in second and other harmonics.

Fig. 23 also shows the relationship between the level of saturation (residual flux) and the duration of the dwell time. In this simulation, we define the dwell time as the fraction of a power cycle during which the magnetizing current is below the saturation level. Therefore, when in linear operation (Point A), the dwell time is one full cycle. For moderate saturation (Point B), the dwell time is about half a cycle. For severe saturation (Point C), the dwell time is about 0.3 cycles. For ultrasaturation, the dwell time eventually reduces to zero, as expected (Point D).

Importantly, Fig. 23 illustrates that the dwell time is a more robust criterion than the second-harmonic content of the differential current alone. For example, when the second harmonic drops below about 15 percent, the dwell time is still about 0.3 cycles. When the dwell time reduces to about one-sixth of a cycle, the second-harmonic content is below 10 percent. Fig. 23 is a theoretical approximation for an arbitrary B-H curve, but it illustrates an important difference between the reduction in the second harmonic and the shortening of the dwell time. We will use this finding in designing the new algorithm in Section VI.

Now we turn our attention to conditions that may lead to ultrasaturation. We have identified two scenarios that may result in elevating the flux to the point of ultrasaturation. They are described in the next subsections.

### B. Unfavorable Transient Flux Components

Refer to Fig. 24, and consider a simplified single-phase transformer with a constant magnetizing inductance of  $L_\mu$  (we can explain this scenario of ultrasaturation assuming a linear magnetizing branch). The transformer is energized from an ideal voltage source  $v_{(t)}$  when the residual flux is at some arbitrary level  $\Psi_R$ . We assume the system ( $S$ ), transformer ( $T$ ), and load ( $L$ ) impedances. They are represented by  $Z_1$  and  $Z_2$  in the model shown in Fig. 24.

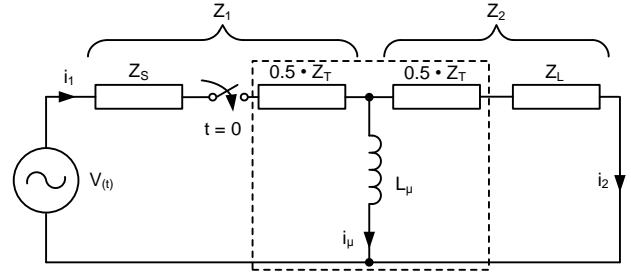


Fig. 24. A simplified model for studying transient flux components during energization.

The linear system of Fig. 24 can be described by the following set of differential equations:

$$\begin{aligned} v &= R_1 i_1 + L_1 \frac{d}{dt} i_1 + \frac{d}{dt} \psi \\ i_1 &= i_\mu + i_2 \\ R_2 i_2 + L_2 \frac{d}{dt} i_2 &= \frac{d}{dt} \psi \end{aligned} \quad (5)$$

Assuming the system voltage is sinusoidal:

$$v_{(t)} = v_m \sin(\omega t + \alpha) \quad (6)$$

and solving these equations for the instantaneous flux, we obtain [3] [4]:

$$\psi = \psi_{AC} \sin(\omega t + \alpha - \Theta_0) + \psi_1 e^{-t/T_1} + \psi_2 e^{-t/T_2} \quad (7)$$

The two exponential components in the total flux have time constants that depend on the parameters of the network in Fig. 24. The magnitudes of the oscillating flux and the decaying components depend on the residual flux, the magnitude and initial angle of the source voltage, and the parameters of the network. Reference [3] provides specific equations for the case of resistive load ( $L_2 = 0$ ).

In general, the sum of the two exponential components in (7) (i.e., the aperiodic flux) can either decay throughout the energization process or increase first and then start to decay. Fig. 25 and Fig. 26 illustrate the two possible situations.

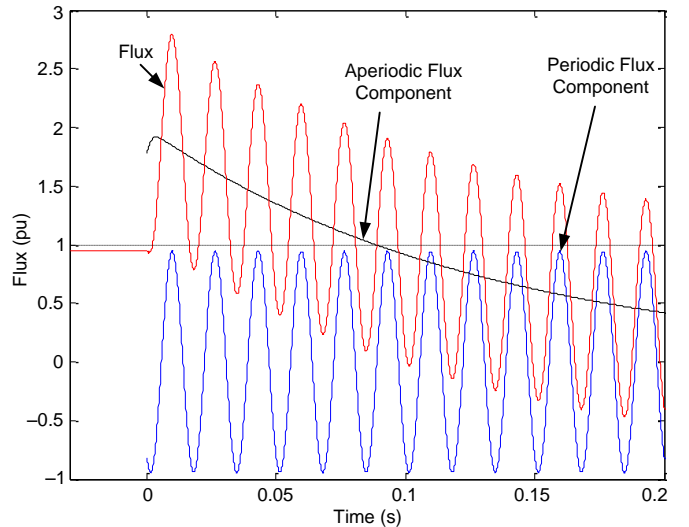


Fig. 25. The flux (red), the periodic component of the flux (blue), and the aperiodic component of the flux (black) for the case with no ultrasaturation despite a very high residual flux.

Fig. 25 presents a case in which the aperiodic flux (black line) shows only a very minor increase and decreases almost from the beginning of transformer energization. The nature of the aperiodic flux makes the solution such that the total flux (red line) is never above the residual flux plus the peak-to-peak magnitude of the periodic flux. As a result, the minimum value of the total flux will be below the saturation level, assuming the residual flux is below the saturation point. Even though the total flux in Fig. 25 started from a very high residual flux of 95 percent of the saturation level, the total flux drops below the saturation level every power cycle. This represents a case of saturation (see Fig. 20 and Fig. 21) but not ultrasaturation.

Fig. 26 shows a case in which the aperiodic flux first increases and starts decaying only after several power system cycles. As a result, the total flux is pushed deep into the saturation region as it follows the aperiodic component. When the flux starts decaying, it does so from a value considerably higher than the residual flux. As a result, the minimum values of the total flux stay above the saturation point for a number of power cycles, resulting in ultrasaturation, previously depicted in Fig. 22. Note that in this example, we assumed a much lower level of residual flux (50 percent of the saturation level) and still the minimum flux is well above the saturation point for several power system cycles.

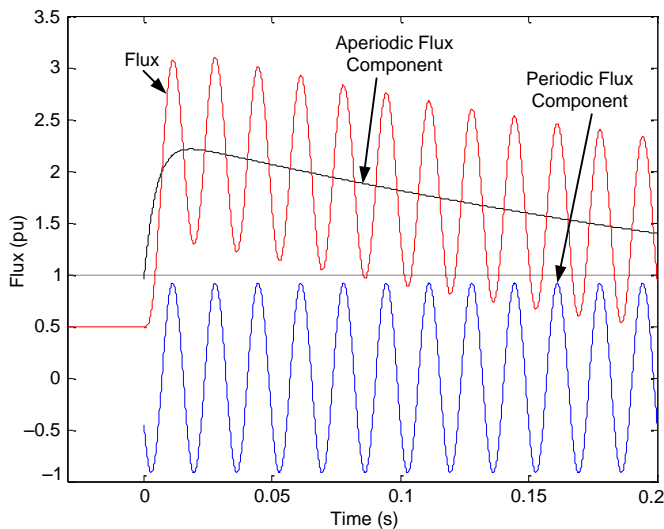


Fig. 26. The flux (red), the periodic component of the flux (blue), and the aperiodic component of the flux (black) for the case of ultrasaturation despite a moderate residual flux.

The following points are worth emphasizing with respect to this scenario of ultrasaturation:

- The phenomenon is caused by unfavorable magnitudes and time constants of the exponential components in the transient flux. This condition, in turn, is associated with a combination of the system, transformer, and load parameters as well as the amount of residual flux.
- The model of Fig. 24 is linear, and the phenomenon derived from it is therefore not caused by nonlinearity of the transformer magnetic core. Of course, the nonlinear nature of the core will alter the actual flux compared with the simplified model of Fig. 24, but the phenomenon is driven by the combination of network parameters and not by nonlinearity of the core.

Even though this scenario of ultrasaturation is not very likely, it may occur if the parameters of the system and transformer happen to align accordingly with the load and residual flux. If cases of ultrasaturation happen only under certain power system configurations (resistive load, consistent values of the load and system impedances), it is worthwhile to examine this scenario as a possible culprit of security deficiencies in transformer differential elements.

### C. Restrike During Energization or De-Energization

Restrike of the disconnecting device could lead to deep levels of saturation and low levels of second harmonic, as we illustrated with field cases in Section III.

Assume some residual flux when the excitation current of an unloaded transformer is interrupted. This residual flux can be low or even have a polarity that helps reduce the inrush current. When the disconnecting device starts conducting, the transformer experiences a typical inrush current. However, when the inrush is interrupted a few cycles later, before the inrush current has a chance to decay, the residual flux is likely to be elevated to its maximum value. This can be best understood by looking at Fig. 6, which shows the core follows the major B-H loop when the flux is decreasing. As a result of developing a higher residual flux when the initial inrush is interrupted, the inrush current on a subsequent restrike is at its maximum dictated by the amount of this maximum residual flux and the source impedance (see Fig. 16 for illustration).

If the restrike continues, the transformer and the CTs will be exposed to a series of inrush current intervals, each having the maximum current magnitude and possibly the same polarity. This possibly subjects CTs to saturation.

#### D. New Transformer Designs

Field experience tends to indicate that newer transformer designs experience ultrasaturation more often, at least as judged by the number of undesired operations of transformer differential relays due to low second-harmonic levels. This problem is attributed to new core materials designed to reduce losses.

The core of the first practical transformer developed in 1885 was made of carbon steel. Later, carbon steel was replaced by silicon steel, and today, most of the power and distribution transformer cores in service are of cold-rolled grain-oriented (CRGO) silicon steel laminations.

The 1980s saw a rapid progress in new magnetic materials called amorphous metals. These Metglas® alloys are made by rapidly cooling molten metal. This production process results in the atoms being located in a disordered structure (similar to glass) and not in a crystalline structure (like silicon steel). This makes amorphous metals easier to magnetize and demagnetize, which directly translates into lower excitation losses in transformers.

Compared with conventional silicon steel transformers, amorphous core transformers have lower core losses, lower excitation current, and higher inrush current and are less noisy. They have lower values of the saturation flux density—about 1.6 T in one particular Metglas (2C 3Si 14B 81Fe) compared with 2 T in one particular CRGO (3Si 97Fe). The new materials are also more expensive and require larger cores. Therefore, they have found applications in smaller transformers used in electronics, power electronics, and some distribution power transformers.

Large power transformers of newer design do not yet apply true Metglas technology. Nonetheless, they use better core materials with benefits over plain silicon steel. New entrants in the field of power transformer manufacturing, such as those in Asia, embrace newer core materials for the competitive advantage of reduced losses.

We offer two explanations as to why newer designs are more susceptible to ultrasaturation, which are the following:

- Lower saturation flux.
- Narrower B-H loops.

Fig. 27 compares a simplified inrush current analysis of the silicon steel type of magnetic material with an improved material. The new material has a lower saturation level, steeper characteristic in the low-flux region (lower excitation current), and flatter characteristic in the saturation region (larger inrush currents). We assumed an oscillating flux with minimum values just above the saturation point of the new material. In this case, the same flux yields ultrasaturation for the new core material (low second harmonic, large inrush current) while it may produce the expected inrush current for the traditional core material (considerable second harmonic, lower inrush current).

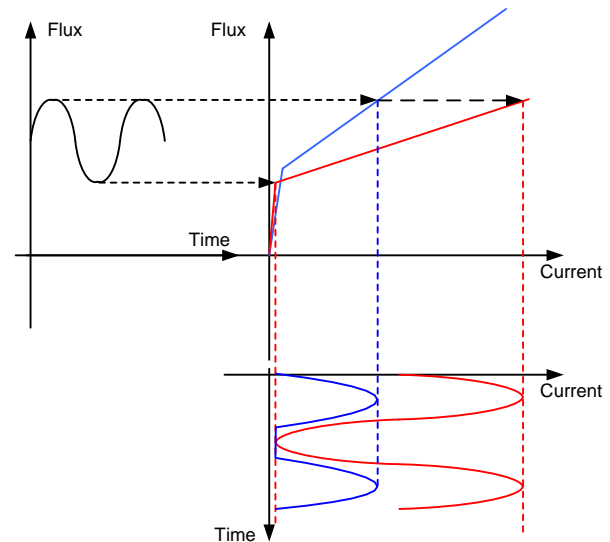


Fig. 27. Impact of the magnetizing characteristic on the inrush current for the same level of flux (blue is a silicon steel type of core material and red is an improved core material).

Fig. 28 compares the major (outer) magnetizing loops of the traditional core material with the material optimized for lower losses. The latter must have a narrower loop because the loop area is related to the level of core losses.

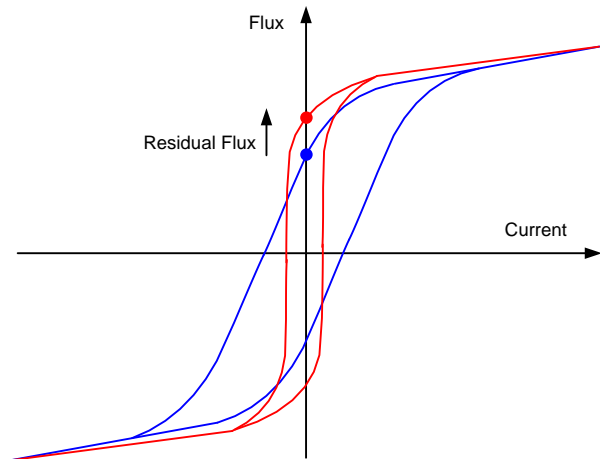


Fig. 28. Impact of the hysteresis loop width on the level of residual flux (blue is a silicon steel type of core material and red is an improved core material).

A narrower loop (which has the same saturation level) crosses the horizontal axis at a higher value, resulting in higher residual flux. Therefore, transformers with improved core material see higher levels of residual flux. This, in turn, makes the saturation deeper and increases the potential of ultrasaturation.

### E. Ultrasaturation of CTs

CTs are subject to the same ultrasaturation phenomenon as power transformers. CT ultrasaturation happens when the oscillating component in the primary current is relatively low while the decaying dc component lasts for a very long time. As a result, the CT flux is driven into the saturation region and stays there permanently as the operating flux-magnetizing current operating point moves only slightly due to the low ac component in the primary current. This scenario is often encountered during remote faults near generators (due to very high source X/R ratio) and during transformer inrush (the oscillating component decays while the dc component can last for a second or longer).

Ultrasaturation of CTs is therefore important in the context of this paper because it may happen during transformer inrush conditions, and when it happens, it alters the shape of the secondary currents measured by the 87T relays.

Consider a typical inrush current as the primary current of a CT, and assume a resistive CT burden. The ratio current multiplied by the burden resistance creates the magnetizing voltage for the CT core (see Fig. 29). The integral of this voltage becomes the flux of the core. Because the current is unipolar, the flux continues to increase. As the flux increases, the CT core draws a larger and larger magnetizing current. The magnetizing current subtracts from the ratio current, shifting the secondary current down. Eventually, when the CT is in ultrasaturation, the secondary current waveform becomes symmetrical.

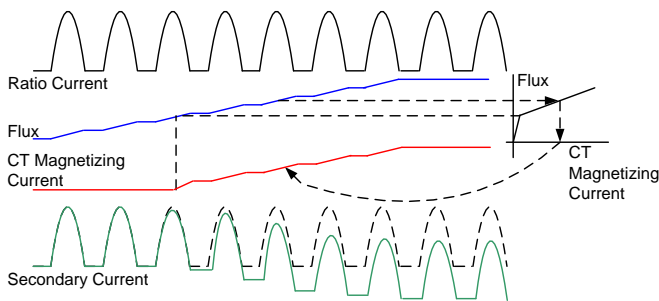


Fig. 29. Explanation of ultrasaturation of a CT.

Prior to CT ultrasaturation, the secondary current reproduces the primary current accurately. At the moment the minimum flux reaches CT saturation level, the CT magnetizing current becomes significant. This current does not oscillate much because the ac component in the primary current is low. As a result, this near-dc magnetizing current reduces the secondary current and eventually makes it nearly symmetrical. After some time, the secondary current does not contain the decaying dc offset. This type of saturation can jeopardize generator, bus, and line differential relays. Reference [5] describes external fault detection logic to solve the problem of protection security during this type of CT saturation.

### F. Inrush Current Characteristics During Ultrasaturation

The following observations can be made based on what we have explained and illustrated so far in this paper:

- Unfavorable residual flux is possible in one or two phases (legs) of a transformer. Therefore, high current values typically occur in two phases while the third phase shows considerably smaller inrush current. As a result, ultrasaturation can happen in one or two phases but not in all three phases (see Fig. 12).
- Ultrasaturation due to unfavorable transient flux is a temporary phenomenon. The transformer pulls out of ultrasaturation in several power system cycles (see Fig. 26).
- Low levels of second harmonic are not caused by transformer vector group compensation. The differential currents, by their very nature, measure the magnetizing currents, and it is the magnetizing currents that exhibit low second-harmonic content. Terminal currents can have different levels of second harmonic; therefore, a given differential current can exhibit low second harmonic depending on how the terminal currents are combined into differential currents per the art of transformer protection (compare Fig. 12 through Fig. 15).
- Using other even harmonics for security during inrush can help marginally but does not guarantee success during ultrasaturation (see Section III). When the core works in the linear second slope region, the current is not distorted, yielding low levels of all harmonics.
- Even though the current is not distorted during ultrasaturation, it is fully offset.
- The dwell-time criterion is effective for deeper levels of saturation as compared with the second-harmonic criterion.
- Ultrasaturation of CTs during inrush is a possibility because of the long-lasting decaying dc component. CT saturation alters the dwell-time periods. A subsidence current pattern is visible in the secondary current. This is expected because the primary current goes to approximately zero for the duration of the dwell time, similar to when the breaker interrupts. As a result of CT saturation, the current within the dwell-time periods departs from zero and becomes slightly tilted (see Fig. 9 and Fig. 10 for examples and Fig. 29 for an explanation).
- The dwell-time periods are aligned in time between the three differential currents in three-leg transformers (see Fig. 10, Fig. 12, and Fig. 14 for examples).

These observations allow us to provide some solutions to the problem of low second harmonic (Section V) and devise a new inrush detection algorithm (Section VI).

## V. SOLUTIONS USING STANDARD 87T ELEMENTS

The large capital cost to purchase and install a transformer, plus the potential for environmental damage and safety risks to staff and the public in the event of a catastrophic transformer failure, leads to the demand for high-speed, sensitive, and highly dependable protection. Conversely, the only means of transferring power between systems operating at different voltage levels is via transformers. Therefore, there is a strong need to avoid removing unfaulted transformers from operation unnecessarily and a demand for a high degree of security in protection as well. These conflicting requirements for security and dependability make the protection of power transformers one of the most challenging application scenarios for protection engineers. The dependability of the protection is generally addressed by applying suitably sensitive settings for the main transformer differential element and by provisioning additional protection elements, such as sudden pressure rise (SPR) and high-set unrestrained differential elements. The overall design of protection schemes for power system transformers is outside the scope of this paper. This section focuses on some specific strategies for improving the security of the percent-restraint transformer differential element for inrush conditions with the phenomenon of ultrasaturation and the issue of potentially low second-harmonic content in the inrush current. None of these solutions is ideal because they require tradeoffs be made between dependability and security and they create different challenges for settings, testing, and operations. One advantage in using a modern microprocessor-based relay with programmable logic and access to comparators of the 87T element is that such options are relatively simple to implement.

### A. Reducing the Second-Harmonic Threshold

After encountering an installation where the second harmonic is a problem, it may be acceptable, at least on a temporary basis until a better solution is available, to reduce the second-harmonic threshold to allow the blocking logic to block at lower harmonic levels or the restraining logic to produce higher restraint from a lower second-harmonic value (increase  $K_2$  and  $M_2$  in Fig. 11). Additionally, the  $M_4$  multiplier in the harmonic restraining scheme can be increased.

This solution is simple in that it does not require any custom logic or special testing. It also retains the per-phase operation of the 87T element and the resulting dependability for faults during inrush conditions. The main disadvantage is a delay or a failure to operate for an internal fault should the CTs saturate and produce harmonics. This is the main reason why protection engineers are normally very hesitant to apply second-harmonic blocking settings lower than 15 percent. Lowering the threshold can be a temporary solution until a relay with a better inrush detection method can be installed, especially if an SPR relay is in place to back up the 87T element.

### B. Riding Through Low Second Harmonic With Time Delay

Another option is to develop custom user logic to block tripping from the differential element for a period of time following the reset of the second-harmonic blocking declaration. For example, the Phase A differential trip could be blocked for 100 milliseconds following the second-harmonic level in the corresponding Phase A differential current falling below the inrush threshold setting. In this case, should the second-harmonic content drop below the inrush blocking threshold for a short period of time due to an ultrasaturation condition, the differential element would be blocked for some period, allowing the transformer to come out of ultrasaturation.

There are three fundamental issues with this particular approach. The first is in determining a suitable length of time to block the differential trip based on the second harmonic falling below the blocking threshold, because there is no way of calculating *a priori* how long an ultrasaturation condition may persist. The second issue arises when a fault occurs after the transformer has been energized but is still in the inrush phase. In this case, the second-harmonic level will likely drop below the inrush blocking threshold; however, the transformer protection will be blocked from tripping for the blocking extension time. The third issue is the need to develop individual custom logic for each manufacturer of transformer relays in use (every manufacturer has its own subtle differences in the way such a scheme is implemented).

### C. Cross-Phase Blocking

Typically, only one phase of the 87T element exhibits low second-harmonic content. This leads to an idea of cross-phase blocking. Fig. 30a presents a one-out-of-three logic (if any phase shows high second-harmonic content, all phases are blocked), and Fig. 30b shows a two-out-of-three logic (if two phases show large second harmonic, the third phase is blocked too).

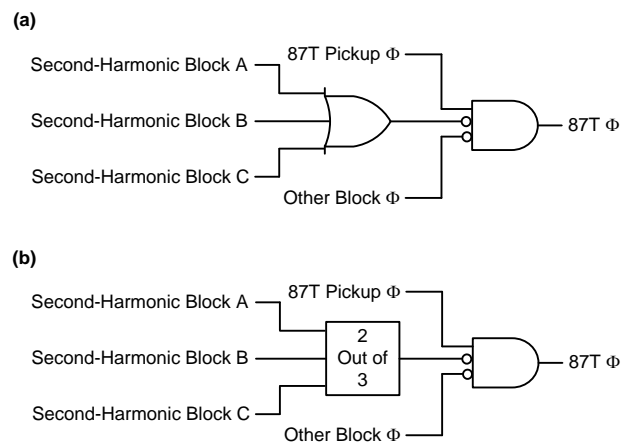


Fig. 30. Cross-phase blocking schemes: one out of three (a), and two out of three (b).  $\Phi$  stands for the phase (A, B, or C).

We should make sure that a phase is allowed to participate in the voting only if its current is non-zero. Current values that are at the noise level can show high second-harmonic ratios and lead the differential element to block spuriously. This can be easily accomplished by checking if the corresponding phase differential signal is greater than the 87T pickup level.

The main concern is dependability for faults during inrush conditions. As shown in the internal fault example of Fig. 35 in the next section, the cross-phase blocking schemes can cause the 87T element to block for an internal fault. Again, this option may be acceptable as a remedial solution if the 87T element is backed up by SPR protection. There is also a practical issue, in that each manufacturer will implement their own cross-blocking logic in a unique way.

#### D. Cross-Phase Blocking With Time Override

We can refine the cross-blocking scheme by allowing it to operate on a per-phase basis but with a time delay and allowing it to operate instantaneously on a cross-phase basis. Fig. 31 shows one possible implementation of this logic.

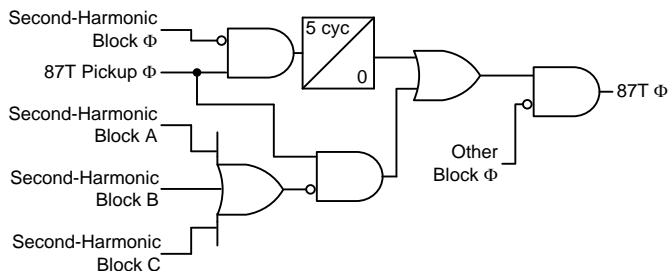


Fig. 31. Cross-phase blocking with a time override.

This scheme works for cases where the second harmonic is low only for some period of time and recovers relatively quickly. The sample five-cycle timer is selected to ride through the low level of the second harmonic. If none of the other phases sees inrush, the timer is bypassed and the element operates without the delay.

#### E. Extra Security Applied Only Upon Energization

We can apply extra security (lower threshold, time delay, cross-phase blocking, or a combination) only for a limited time after energizing the transformer.

One possible solution is presented in Fig. 32. In this scheme, we use the restraining current to detect a de-energized transformer. If the restraining current is below some threshold (0.08 pu, for example) for some time (10 seconds, for example) in all three phases, we declare the transformer de-energized and apply more secure 87T settings or logic. When the transformer is energized, the dropout (DPO) timer continues to force the more secure settings or logic. Therefore, the DPO timer should be set longer than the duration of the inrush current (2 to 3 seconds, for example). After the DPO timer expires, the scheme reverts to normal 87T settings or logic.

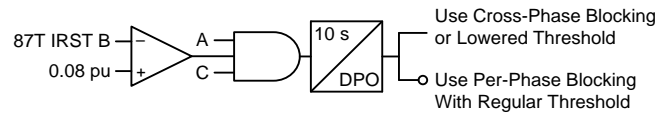


Fig. 32. Applying secure settings only upon energization.

The logic in Fig. 32 also asserts for an unloaded transformer. To improve security, this scheme can be modified to include voltage or isolator status, if available.

Again, there is a potential loss of dependability for faults during energization as well as the disadvantages of more complex testing and manufacturer-specific logic implementation that needs to be developed.

#### F. Utility Requirements for Transformer Differential Supervision

In order to be able to maximize both the dependability and security of transformer protection, ideally the decision to block a given phase of a differential element from operating should be based solely on the compensated differential current for that phase. In other words, the presence of second harmonics in the Phase A differential current should successfully block the operation of the Phase A differential element only. Conversely, if the transformer is energized with a fault on Phase A, then the presence of high second-harmonic content in Phase B and Phase C should not prevent the Phase A differential element from tripping.

Also, the blocking decision should be able to be reset quickly in the event that a transformer fault occurs during transformer energization, even if an ultrasaturation condition exists. This includes situations where CT saturation can occur and introduce some amount of second-harmonic content into the differential current.

## VI. A NEW METHOD TO ADDRESS INRUSH DURING ULTRASATURATION

This section describes an improved inrush detection algorithm to address the stated utility requirements and to cover the cases of very low second harmonic, as well as a new algorithm to accelerate operation during internal faults. We based the new inrush detection algorithm on the dwell-time principle: the existence of periods of small and flat currents in every cycle of a true inrush current. Moreover, these dwell-time intervals are aligned in the case of a three-phase, three-legged transformer (a prevailing design for economical and size reasons; we discuss other core types later in this section).

The last observation deserves an explanation and some clarification. Consider a three-legged power transformer. In this design style, the flux in all three legs must sum to zero at any given time because the leakage flux is negligible. This is illustrated in Fig. 33.

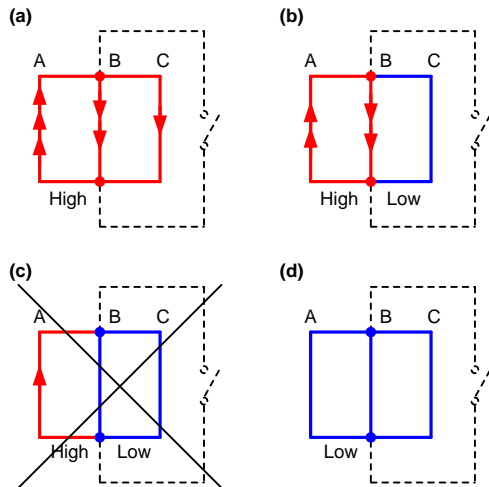


Fig. 33. Possible patterns of saturation in a three-legged transformer design. The arrows represent flux. Red is high flux above the saturation level; blue is low flux below the saturation level.

Fig. 33a illustrates a period of time when the Leg A flux is so high that the returning flux in Legs B and C is also above the saturation level. In this case, all three legs are saturated and all three magnetizing (differential) currents are high (compare with Fig. 10).

Fig. 33b illustrates a period in time when the Leg A flux decayed to the point that the returning flux in Leg C is below the saturation level. As a result, the A and B flux values are equal and they must be of opposite directions. Comparing with Fig. 10, this period of time represents a situation where one magnetizing current is low and the two other currents are still significant, equal in magnitude, and out of phase.

Note that the situation of Fig. 33c is not possible. We cannot have a significant flux in Leg A with no flux in Legs B and C. Therefore, the case of Fig. 33b can only progress (as Leg A pulls further out of saturation) into the case of Fig. 33d. This means that as Leg A pulls out of saturation, the companion Leg B pulls out of saturation as well. As a result, all three legs are out of saturation at the same time. Comparing with Fig. 10, this is a period of time when all three currents are near zero.

Because the transformer is energized from a symmetrical ac source, the pattern of Fig. 33a, b, and d keeps repeating (see Fig. 10). As a result, the pattern of Fig. 33d is guaranteed to repeat itself every power cycle.

The differential currents are combinations of terminal currents as per the art of transformer differential protection [1]. During dwell times, all the inrush currents are zeros. Combining zero values in any fashion still returns zero values. We therefore can be assured that the dwell-time intervals are aligned not only between the phases of the terminal currents but also between the three phases of the differential currents.

The situation is different in single-phase units. In this case, the dwell-time intervals appear independent of each other because the fluxes in all the single-phase cores are independent (the same applies to the four- and five-legged core designs).

### A. A New Dwell-Time-Based Algorithm

Fig. 34 presents a simplified block diagram of the new inrush detection algorithm for three-legged transformers. Instantaneous values of the differential currents in all three phases (87T IDIF A, 87T IDIF B, and 87T IDIF C) are the inputs to the algorithm, and the Boolean flag INRUSH is the output (when asserted, the differential element shall be blocked). Note that the algorithm uses information in all three phases but asserts a single output flag. We discuss this observation later.

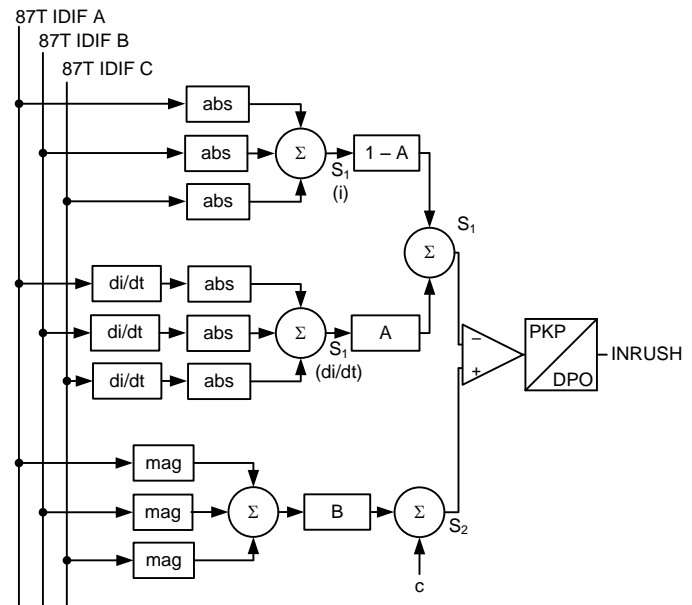


Fig. 34. Simplified block diagram of the new inrush detection algorithm.

The algorithm is executed on a sample-by-sample basis and works as follows:

- The absolute values of the instantaneous differential current values in all three phases are added to form the  $S_1(i)$  signal. During inrush conditions, this signal is very low for the duration of the dwell-time periods because all three differential currents exhibit their dwell times at the same time. During internal fault conditions, this signal is high and reflects the fault current. If CT saturation occurs during inrush, the differential currents during dwell-time periods start departing from zero and the signal starts to increase slightly with time. Therefore, we introduce the second measure of the dwell-time pattern as follows.
- The instantaneous differential signals are differentiated ( $di/dt$ ). Because the inrush currents during dwell-time periods are flat, the output of the derivative is ideally zero. The absolute values of the derivatives are taken next, and all three phases are summed to form the  $S_1(di/dt)$  signal. Because all three inrush currents are flat during dwell-time periods, this signal is very low during inrush conditions during the dwell-time periods. However, because of CT ultrasaturation, this signal may increase as well, but at a much lower rate compared with the  $S_1(i)$  signal.

- The  $S_1$  (i) and  $S_1$  (di/dt) signals are added with the weighting factor  $A$  (for the purpose of demonstration, a value of  $A = 0.5$  is used although this value could be adjusted if required based on transformer characteristics). The resulting signal  $S_1$  is low during the dwell-time periods and high during internal faults. This signal is quite resilient to CT saturation during inrush. Even though the secondary currents depart from zero during dwell-time periods due to CT saturation, they are still relatively flat. We can increase the resilience of the algorithm to CT saturation during inrush by increasing the value of  $A$ .
- During inrush the  $S_1$  signal is very low once a cycle for the duration of the dwell time. The comparator checks the level of  $S_1$ . If this signal is low for the duration of the pickup time (PKP), then INRUSH is asserted and maintained for one more power cycle (DPO). The dropout timer is required to wait for the next dwell-time period in order to maintain reliable inrush detection.
- The pickup timer (PKP) is set to the desired level of dependability in detecting inrush. For example, it can be set to one-sixth (or even as low as one-eighth) of the power cycle, allowing it to cope with cases of the second harmonic as low as 10 percent and below (see Fig. 23).
- The comparator uses an adaptive reference for the  $S_1$  signal. The magnitudes of the differential current are measured and added together.  $S_2$  is formed as a portion of the sum of the magnitudes (multiplier  $B$ ) plus a constant,  $C$ .  $S_1$  being less than  $S_2$  declares the  $S_1$  signal low and thus signifies the dwell-time period. For the purpose of demonstrating the algorithm operation,  $B$  is 0.1 and  $C$  is 0.1 pu.

Fig. 35 through Fig. 37 illustrate operation of the new algorithm using an inrush case recorded in the field with a simulated fault current superimposed on the inrush waveform. (In Fig. 35, the fault was added at about 72 milliseconds.) This case is a realistic representation of an internal fault that develops during transformer energization. We expect the algorithm to block in the first 72 milliseconds of inrush (protection security) and deassert shortly afterward (protection dependability).

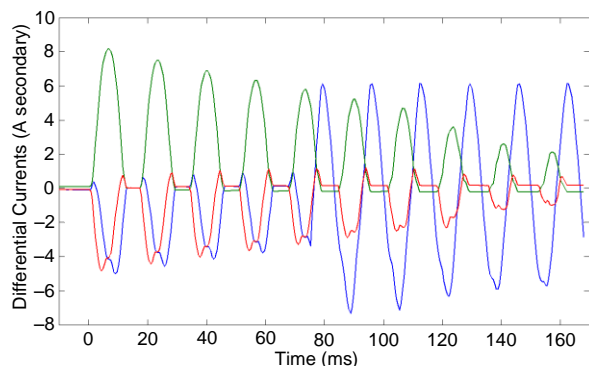


Fig. 35. Differential currents for an internal fault during inrush conditions.

Fig. 36 shows some key internal signals of the algorithm. As expected during inrush conditions, the  $S_1$  (i),  $S_1$  (di/dt), and  $S_1$  signals are low for the duration of the dwell-time periods. After the internal fault happened in the blue phase, the  $S_1$  dwell-time intervals have practically disappeared from the  $S_1$  signal, though the other two phases are true inrush currents with clearly visible dwell-time periods.

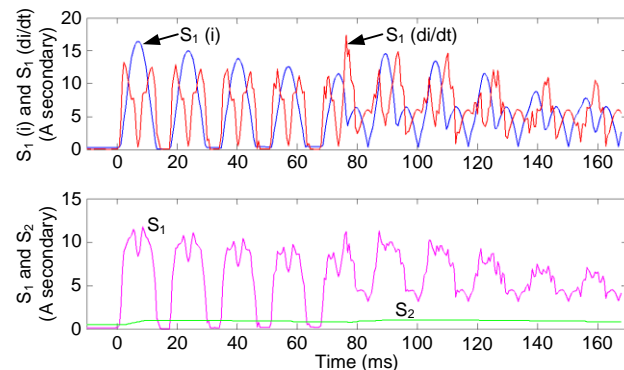


Fig. 36.  $S_1$  (i) (blue),  $S_1$  (di/dt) (red),  $S_1$  (magenta), and  $S_2$  (green) signals for the case of Fig. 35.

The  $S_1$  signal drops repetitively below the  $S_2$  signal during inrush and stays consistently above the  $S_2$  signal after the internal fault (Fig. 36, bottom). This means that during inrush conditions, the PKP timer picks up and maintains a solid INRUSH assertion. The last dwell-time interval in the  $S_1$  signal occurs at about 65 milliseconds. If it was not for the internal fault, the next interval would occur at about  $65 + 17 = 82$  milliseconds. The DPO timer expires after about one cycle (around 82 milliseconds), and because there is no new dwell-time period present, the scheme resets, allowing the differential element to trip.

When applied to single-phase units, the scheme needs to be phase-segregated [i.e., using the phase-segregated signals  $S_1$  (i),  $S_1$  (di/dt),  $S_1$ , and  $S_2$ ]. This is because the dwell-time intervals are not aligned in time in single-phase or four-legged core design transformers. In a transformer built with single-phase units, the flux in each core is independent and the three cores go in and out of saturation independently. We can say that one instance of the new algorithm is required per each core of the transformer (understanding that four- or five-legged cores are equivalent to three separate single-phase cores). This is logical because the new algorithm monitors the core inrush condition.

The new scheme is simple and intuitive. It does not require any user settings because the four design constants ( $A$ ,  $B$ ,  $C$ , and PKP timer) can be selected for a wide range of transformers. Of these factory constants, only the PKP time may be of some interest to users because it dictates the balance between protection security (short delay equals declaring inrush for short dwell times) and dependability (longer delay equals declaring a fault if dwell times are too short).

The new scheme improves the performance of previous implementations of the dwell-time principle by using a derivative of the current in addition to the current itself (to improve performance for CT saturation) and by correlating

information from all three phases. Requiring that all three phases simultaneously display their dwell intervals increases security of the inrush detection scheme (i.e., prevents it from declaring an inrush during internal faults with heavy CT saturation). It is important to notice that the method is not a cross-phase method: if any of the phases stop exhibiting dwell times, the scheme will deassert (see Fig. 36).

The scheme shares, however, one common disadvantage with traditional second-harmonic blocking—it takes approximately one cycle to deassert the blocking signal after an internal fault during inrush. In the case of second-harmonic blocking, the delay results from the transient response of the second-harmonic filters (see Fig. 13). In the new method, the delay is intentional and set by the DPO timer of about one cycle.

In the next subsection, we propose a bidirectional instantaneous differential overcurrent element to speed up operation for internal faults.

### B. Bidirectional Differential Overcurrent Element

The inrush current, if high, is practically unipolar. It becomes more symmetrical as the inrush decays into a steady-state excitation current (see Section II).

Fig. 37 shows the differential current of Fig. 35 superimposed on two thresholds. Note that during inrush conditions (the first 72 milliseconds), the current is negative and it repeatedly crosses the negative threshold (the dashed blue line in Fig. 37). At the same time, however, it does not cross the symmetrically placed positive threshold (the dashed red line).

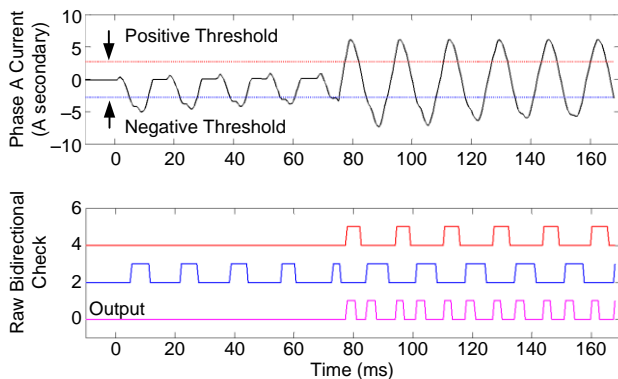


Fig. 37. Fault current of Fig. 35 compared with positive (red) and negative (blue) thresholds. The magenta flag represents the output of the element.

Note, however, that when the internal fault happens, the current crosses the negative threshold; shortly afterwards, it crosses the positive threshold; and so on. We use this observation to devise a new protection element as depicted in Fig. 38.

In this scheme, the instantaneous differential current (87T DIF) is compared with the positive (+D) and negative (−D) thresholds. If the current is above the positive threshold for a short duration of time (PKP timer), a window is opened with the DPO timer to see if the current decreases to below the

negative threshold. If it does, the current must be symmetrical, and therefore, it is not an inrush current. Mirror logic is used for the negative polarity—if the current is confirmed significantly negative and shortly afterward it becomes positive, the inrush hypothesis is ruled out.

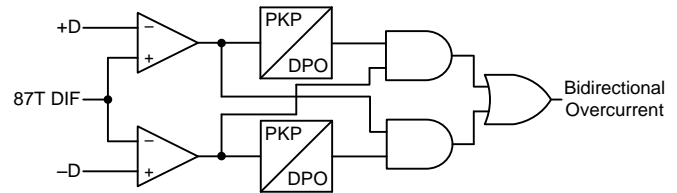


Fig. 38. Principle of operation of the bidirectional differential overcurrent element.

The PKP timer is introduced for security (one-eighth of a cycle, for example). The DPO timer is set to about one-third to one-half of a cycle.

The magenta line in Fig. 37 is the output of the scheme. As we can see, the element asserts at about 78 milliseconds (the fault occurred at about 72 milliseconds). This response time of about 6 milliseconds to a fault occurring during inrush is considerably faster compared with the reset time of about one cycle of any inrush detection method (second-harmonic blocking or the new method presented in the previous subsection).

Owing to its bidirectional check, this element does not have to be set very high to ensure security during inrush or external faults with CT saturation. As a result, it has a chance to respond to a larger percentage of internal faults compared with the traditional unrestrained differential element.

### C. Application Considerations

The new method of detecting inrush conditions can be used alone, or it can be combined with either harmonic blocking or harmonic restraining. Moreover, we can apply various hybrid schemes similar to those described in Section V.

The new bidirectional instantaneous differential overcurrent element can be applied to unblock the differential element with the intent to accelerate the operation of the traditional differential element, or it can be used directly for tripping in a manner similar to the traditional unrestrained differential element (see Fig. 39). The directly tripping application (BI-DIR OC 2 initiating a trip without any through-fault restraint or harmonic blocking) may use slightly higher settings for security, but it still can be much more sensitive compared with the element that responds to the filtered magnitude of the differential current.

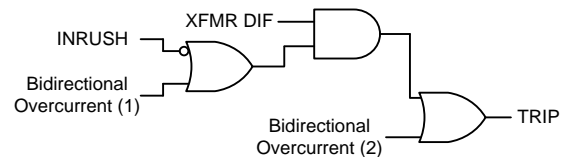


Fig. 39. Applications of the new elements.

## VII. CONCLUSION

This paper reviews magnetizing inrush conditions in power transformers. Special emphasis is put on the cases of very deep saturation (known as ultrasaturation) when not only the maximum but also the minimum flux is at or above the saturation level.

Several conditions that can lead to ultrasaturation are discussed and illustrated.

Ultrasaturation can happen when energizing a loaded transformer due to an unfavorable transient flux in the core. This transient flux can push the operating point deeply into the saturation region of the B-H curve for a very large fraction of the power cycle, to the extent that the core goes out of saturation for very short period of time in each cycle, or not at all.

Inrush during restriking of a disconnecting device is another case that can lead to deep saturation.

Deep or ultrasaturation is more likely to happen in newer transformers due to their improved core material, but it can also happen in older units.

Deep saturation results in lower levels of second harmonic in the differential currents and can lead to misoperation of differential relays due to insufficient harmonic blocking or restraining action.

Inrush current contains slowly decaying dc components, and therefore, it stresses the protection CTs. This is especially true during restrikes because each time the transformer is re-energized, the current is not only unipolar but also high. Ultrasaturated CTs distort the secondary current, potentially creating more problems for protective relays.

Several simple solutions are proposed to remediate the problem of low second harmonic during inrush (cross-phase blocking, temporary reduction in the blocking threshold, and so on). These methods gain extra protection security at the expense of dependability.

A new method is presented based on the dwell-time principle, using information from all three phases as well as the current derivatives. The new method allows blocking for very deep core saturation without jeopardizing protection dependability. As such, the new method is considerably better than the second-harmonic principle.

Another new method is presented to accelerate detection of internal faults versus inrush. The bidirectional instantaneous differential overcurrent element allows faster inrush unblocking. It can also be used for direct tripping. The element can operate in half a cycle, even at relatively low internal fault current levels.

## VIII. REFERENCES

- [1] B. Kasztenny, M. Thompson, and N. Fischer, "Fundamentals of Short-Circuit Protection for Transformers," proceedings of the 63rd Annual Conference for Protective Relay Engineers, College Station, TX, March 2010.
- [2] A. Guzmán, H. Altuve, and D. Tziouvaras, "Power Transformer Protection Improvements With Numerical Relays," proceedings of the CIGRE B5 Colloquium, Calgary, Canada, September 2005.

- [3] X. N. Lin and P. Liu, "The Ultra-Saturation Phenomenon of Loaded Transformer Energization and Its Impacts on Differential Protection," *IEEE Transactions on Power Delivery*, Vol. 20, Issue 2, April 2005, pp. 1265–1272.
- [4] A. Wiszniewski, W. Rebizant, D. Bejmert, and L. Schiel, "Ultrasaturation Phenomenon in Power Transformers—Myths and Reality," *IEEE Transactions on Power Delivery*, Vol. 23, Issue 3, July 2008, pp. 1327–1334.
- [5] E. O. Schweitzer, III, N. Fischer, and B. Kasztenny, "A Fresh Look at Limits to the Sensitivity of Line Protection," proceedings of the 37th Annual Western Protective Relay Conference, Spokane, WA, October 2010.

## IX. BIOGRAPHIES

**Steven Hodder** received a bachelor of engineering degree (first class standing) in electrical engineering from Lakehead University in Thunder Bay, Ontario, in 2000. He has over ten years of experience in the power system protection and control field and is currently a senior protection and control specialist in the engineering standards and new technology development department of Hydro One Networks, Inc., specializing in transmission and substation protection design. Steven is a member of the IEEE Power and Energy Society (PES) and Standards Association (SA).

**Bogdan Kasztenny** is the R&D director of technology at Schweitzer Engineering Laboratories, Inc. He has over 23 years of expertise in power system protection and control, including ten years of academic career and ten years of industrial experience, developing, promoting, and supporting many protection and control products. Bogdan is an IEEE Fellow, Senior Fulbright Fellow, Canadian representative of CIGRE Study Committee B5, registered professional engineer in the province of Ontario, and an adjunct professor at the University of Western Ontario. Since 2011, Bogdan has served on the Western Protective Relay Conference Program Committee. Bogdan has authored about 200 technical papers and holds 20 patents.

**Normann Fischer** received a Higher Diploma in Technology, with honors, from Witwatersrand Technikon, Johannesburg in 1988, a BSEE, with honors, from the University of Cape Town in 1993, and an MSEE from the University of Idaho in 2005. He joined Eskom as a protection technician in 1984 and was a senior design engineer in the Eskom protection design department for three years. He then joined IST Energy as a senior design engineer in 1996. In 1999, he joined Schweitzer Engineering Laboratories, Inc. as a power engineer in the research and development division. He was a registered professional engineer in South Africa and a member of the South Africa Institute of Electrical Engineers. He is currently a senior member of IEEE and a member of ASEE.

**Yu Xia** received a B.Sc. from the University of Science and Technology of China, Hefei, Anhui, China in 2008 and a Ph.D. from the University of Idaho in 2013. He joined Schweitzer Engineering Laboratories, Inc. in 2011 and holds the position of power engineer in the research and development division. He was an intern at the Chinese Academy of Sciences, Shanghai, in 2007. He is a member of IEEE.